INTERNATIONAL JOURNAL OF HYDROGEN ENERGY 39 (2014) 5899–5905

Available online at www.sciencedirect.com

ScienceDirect

journal homepage: www.elsevier.com/locate/he

A new model for the prediction of oxygen interference in hydrogen storage systems

A. Sigal [a], M. Villarreal [b], M.I. Rojas [b,*], E.P.M. Leiva [b]

[a] Facultad de Matemática, Astronomía y Física, Universidad Nacional de Córdoba, Ciudad Universitaria, 5000 Córdoba, Argentina

[b] INFIQC – Departamento de Matemática y Física, Facultad de Ciencias Químicas, Universidad Nacional de Córdoba, Ciudad Universitaria, 5000 Córdoba, Argentina

ARTICLE INFO

Article history:
Received 3 October 2013
Received in revised form
23 January 2014
Accepted 26 January 2014
Available online 18 February 2014

Keywords:
Hydrogen storage
Absorbent contamination
Molecular dynamic simulations

ABSTRACT

A new model is developed to analyze oxygen interference in hydrogen storage materials. It is based on the competitive adsorption isotherm between the two gases, with the parameters fitted from molecular dynamic simulations. The model is applied to a system consisting of graphene sheets separated by different distances. For a gas-phase mixture of hydrogen (99.9%) and oxygen (0.1%) in interaction with porous graphite of 6.5 Å (optimum size) it can be observed that after 50 cycles of charging/discharging the blocking of active sites of the material by oxygen is ~10%, due to progressive pollution of the system by oxygen. The model presented here may easily be extended to other systems of interest, involving other blocking species or adsorbent materials.

1. Introduction

Hydrogen appears as one of the most promising candidates for being used as a fuel, since it can be obtained from renewable sources and its energy conversion does not produce pollution. It also has the largest energy density out of all combustible materials known today (three times greater than fossil fuels), so that it is likely to gain ground in the world energy mix [1].

Storage remains the bottleneck in the application of hydrogen as an energy carrier, which is necessary to solve in an efficient and compact way. This represents the major technical difficulty for practical applications [2]. The alternatives for hydrogen storage can be divided into three groups: as a compressed gas, as a liquid (at −250 °C), or adsorbed on solid state materials (metal hydrides or carbonaceous materials).

Carbon-based materials present many advantages: low cost, great surface area, low weight, quick and reversible adsorption/desorption process, and thermodynamic stability. Nowadays, the volumetric and gravimetric densities of hydrogen storage on these systems are not yet suitable for mobile applications under normal temperature and pressure conditions [3].

Recently, there have been many efforts to improve significantly the hydrogen storage capacity of different carbonaceous materials such as activated carbons, carbon nanotubes, and porous graphite [4].

In an attempt to improve the storage capacity of carbonaceous materials, have been decorated with different metals [5]. However, although theoretical studies suggest that hybrid materials would be promissory for storage purposes; experiments did not match theoretical predictions [6].

* *Corresponding author.* Tel./fax: +54 351 5353853.
E-mail addresses: mrojas@fcq.unc.edu.ar, marianarojas65@gmail.com (M.I. Rojas).
0360-3199/$ – see front matter
http://dx.doi.org/10.1016/j.ijhydene.2014.01.175

In recent studies we found that oxygen interference reduces the efficiency of hydrogen storage [7–9] of metal-decorated carbonaceous systems, due to oxygen chemical blocking or oxidation of the metal decoration. Although oxygen in the gas phase can be evacuated until reaching ultra-high-vacuum (UHV) conditions, the remaining molecules present in the gas phase are capable of reducing the efficiency and durability of the materials.

On the other hand, a methodology widely used to generate hydrogen is via water electrolysis. During hydrogen production through Polymer Electrolyte Membrane Water Electrolyzers [10,11] some oxygen produced in the anode may permeate through the Nafion membrane towards the cathode where hydrogen is produced, polluting the hydrogen generation.

Oxygen interacts strongly with the metallic decoration; however, after studying a set of different systems, we found that the most promising metals are Ni, Pd and Pt [8]. Considering manufacturing costs, nickel appears as the most convenient option. The application of a mechanical statistical model allowed studying the effect of the partial pressures of hydrogen and oxygen, suggesting that some of the present systems could work if oxygen access to the surface is suppressed by using a suitable gas-selective porous design. Then, the challenge is to find a way of eliminating oxygen interference. As the oxygen molecule is larger than the hydrogen one, it appears as possible to avoid access of the former to the surface by means of nanoporous surfaces with an optimized pore size, allowing hydrogen access and restricting oxygen entrance sterically [12–14].

Since the last decade, much research work has been devoted to optimize pore size of carbonaceous materials, in order to improve hydrogen adsorption capacity from the gas phase at normal pressures and ambient temperature [15,16]. Other articles have considered hydrogen adsorption on carbonaceous materials with narrow homogeneous porosities and its dependence on the pore size [12–14,17–22].

In the present paper, we employ a graphite porous material to study hydrogen and oxygen adsorption by means of Molecular Dynamics simulations in realistic conditions. We analyze the optimum pore size for favoring hydrogen adsorption and consider the response of the system to oxygen adsorption. By means of heuristic fitting of the adsorption isotherms, we take into account the different adsorption/desorption cycles, analyzing contamination or aging of the material with the number of charge/discharge cycles.

2. Model and computations

2.1. Molecular dynamics simulation

Molecular dynamics simulations were performed with the program GROMACS. We set a graphitic absorbent consisting of eight 6.39 nm × 4.18 nm (1020 carbon atoms per sheet) graphene sheets parallel to the x-y plane. Fig. 1 shows a snapshot of the MD configuration obtained at 300 K and under equilibrium conditions for hydrogen adsorption on porous graphite. The positions of the plates were fixed at several separations to study hydrogen and oxygen adsorption for different pore sizes. Then, we enlarged the box up to 20 nm to introduce the adsorption gases.

The simulations were carried out with constant volume and constant temperature (NVT ensemble). The v-rescale coupling was used to maintain a stable temperature around ambient temperature, and the LINCS algorithm was used to constrain molecule bonds.

For a given pore size, an amount of hydrogen or oxygen molecules was introduced in the simulation box initially, so that the resulting gas density in the graphite-free volume (the area of the box farthest from graphite), corresponded to a saturation pressure in the adsorption isotherms to be obtained. Then different numbers of molecules were progressively removed, allowing construction of the adsorption curves at lower pressures.

To calculate the equilibrium pressures of the system and the adsorbed gas, we previously obtained the density vs. pressure curve for a pure gas, using Berendsen semi-isotropic coupling to keep temperature and the different pressures stable. The equilibrium pressure values were calculated from the polynomial fitting of this curve, collected during 2.2 ns, after 1 ns of system equilibration.

The parameter for H–H and O–O intermolecular interactions were fitted from pressure-density experimental data reported by NIST (National Institute of Standards and Technology) [23]. The Lennard–Jones potentials between the hydrogen (oxygen) molecules with the carbon substrate were

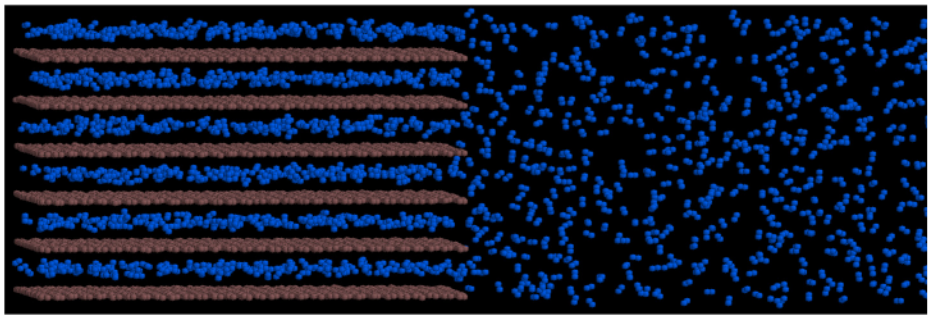

Fig. 1 – Hydrogen adsorption on porous graphite. Molecular dynamics configuration obtained at 300 K and under equilibrium conditions. Brown, C; blue, H.(For interpretation of the references to color in this figure legend, the reader is referred to the web version of this article.)

fitted from PM6-DH2 semiempirical calculations with Van der Waals interactions [24,25] and listed in Table 1.

2.2. Cycling model

In the practical performance of a hydrogen storage system, the porous graphite storage media would be exposed to a mixture of hydrogen and oxygen, and it would also undergo numerous charge/discharge cycles, between a highest charging pressure, P_c, and a lowest discharge pressure, P_d. These pressure values were 200 bar and 1 bar respectively. It is the purpose of the present section to analyze the behavior of the storage media with respect to contamination by oxygen, here assumed as the main interferent for hydrogen storage. We will set up a model based on the results of our MD simulations in order to find out to which extent storage capacity is reduced along the cycling sequence of the container. As pointed out by Bénard et al. [26], a practical model for microporous adsorbents must have a minimal number of parameters and it must allow a straightforward interpretation in terms of the physical properties of the system. Despite its shortcomings, the Langmuir model has been found highly satisfactory to describe the behavior of weakly interacting, supercritical adsorbates, since it provides a simple description of the monolayer filling [26]. This will be our current choice.

Let us denote with γ_{H_2} the hydrogen purity of the gas mixture introduced into the tank in each cycle. We will assume that 90% of the volume of the storage reservoir is filled with the adsorbing material, while the remaining 10% stays as dead volume, denoted with V. While this is a somewhat arbitrary choice and depends on the construction details of the storage device, it is of the order of the magnitude of those found in tanks using hydrogen storage alloys [27].

At a given charge/discharge cycle, the total number of hydrogen $n^T_{H_2}$, and oxygen $n^T_{O_2}$ molecules is given by:

$$n^T_{H_2} = n^g_{H_2} + n^s_{H_2}, \quad n^T_{O_2} = n^g_{O_2} + n^s_{O_2} \tag{1}$$

where $n^g_{H_2}$ and $n^g_{O_2}$ are the number of hydrogen and oxygen molecules in the gas phase respectively, and $n^s_{H_2}$ and $n^s_{O_2}$ are those in the adsorbed phase.

Hydrogen purity allows writing the following equality for the first charging cycle:

$$\frac{n^T_{H_2}}{n^T_{H_2} + n^T_{O_2}} = \gamma_{H_2} \tag{2}$$

While for all cycles the sum of partial pressures of hydrogen and oxygen gives the total pressure:

$$\frac{n^g_{H_2} RT}{V} + \frac{n^g_{O_2} RT}{V} = P \tag{3}$$

Table 1 – Lennard–Jones parameters used in the present simulations.

	ε (kJ/mol)	σ (nm)
C–C	0.293	0.355
H–H	0.093	0.268
O–O	0.420	0.300
C–H	0.230	0.305
C–O	0.440	0.328

where, for the sake of simplicity, we have assumed ideal gas behavior. This assumption is reasonable because we are considering gas storage at room temperature and under these conditions a fairly linear behavior between pressure and density is found in the pressure range considered for the charge/discharge cycles [23].

In the adsorbed phase, the number of sites occupied by hydrogen and oxygen, according to the Langmuir isotherm for competitive adsorption are:

$$n^s_{H_2} = \frac{\alpha_{H_2} P_{H_2} N_T}{1 + \alpha_{H_2} P_{H_2} + \alpha_{O_2} P_{O_2}}, \quad n^s_{O_2} = \frac{\alpha_{O_2} P_{O_2} N_T}{1 + \alpha_{H_2} P_{H_2} + \alpha_{O_2} P_{O_2}} \tag{4}$$

where N_T denotes the total number of adsorption sites in the adsorbent. N_T is the sum of the empty sites n_V, the sites occupied by hydrogen $n^s_{H_2}$, and the sites occupied by oxygen $n^s_{O_2}$ according to:

$$N_T = n_V + n^s_{H_2} + n^s_{O_2} = \text{constant}. \tag{5}$$

α_{H_2} and α_{O_2} are a measure of the affinity of the adsorbent of hydrogen and oxygen respectively.

Assuming that the charging process is fast enough to prevent oxygen and hydrogen molecules on the adsorbent from exchanging with the gas source generating the charging process, the new pressure upon loading of the tank will be given by:

$$P_c = \Delta P_{H_2} + \Delta P_{O_2} + P, \quad \frac{\Delta P_{H_2}}{\Delta P_{H_2} + \Delta P_{O_2}} = \gamma_{H_2} \tag{6}$$

where ΔP_{H_2} and ΔP_{O_2} are the variations of the hydrogen and oxygen pressures respectively, in the charging process, which are given by $\Delta P_{H_2} = \Delta n_{H_2} RT/V$ and $\Delta P_{O_2} = \Delta n_{O_2} RT/V$, where Δn_{H_2} and Δn_{O_2} are the corresponding in number of gas moles introduced in the charging process. In other words, the pressure of the external source is equilibrated with that provided by the gas molecules previously existing in the dead volume plus that delivered by the oxygen and hydrogen molecules newly coming into the system.

Through mass balance and corresponding Langmuir isotherms, we have after equilibration of the gas with the carbonaceous adsorbate:

$$P_{H_2} + \Delta P_{H_2} + \frac{\alpha_{H_2} P_{H_2}}{1 + \alpha_{H_2} P_{H_2} + \alpha_{O_2} P_{O_2}} \frac{N_T RT}{V} - P^{c.Eq}_{H_2} + \frac{\alpha_{H_2} P^{c.Eq}_{H_2}}{1 + \alpha_{H_2} P^{c.Eq}_{H_2} + \alpha_{O_2} P^{c.Eq}_{O_2}} \frac{N_T RT}{V} \tag{7}$$

where $P^{c.Eq}_{H_2}$ is the charge pressure in the gas phase when the system reaches equilibrium. With a similar equation for oxygen, the new total pressure in the charge balance can be computed from:

$$P_{c.Eq} = P^{c.Eq}_{H_2} + P^{c.Eq}_{O_2} \tag{8}$$

We consider an infinitely slow discharge of the gas, so that at each differential step a quantity $dn^{out}_T = dn^{out}_{H_2} + dn^{out}_{O_2}$ exits the tank. Every differential step leads to a new equilibrium, so that the container is discharged reversibly. For each of these steps, the intermediate partial pressures are computed from the above equations until the desired 1 bar discharge pressure P_d is reached.

With these values, we perform the calculations of the second cycle for loading/unloading, and so forth, until reaching the nth cycle.

All the notation parameters of the model are listed in Table 2.

3. Results and discussion

3.1. Hydrogen storage

In order to optimize graphite pore size for hydrogen storage, we first performed molecular dynamics simulations at 300 K for hydrogen adsorption onto the system considering pore sizes within a [5.5 Å, 10 Å] range. The reason for the lower limit is that, below this size, hydrogen was found to be unable to penetrate into graphite layers. The upper limit corresponds to the formation of two adsorption layers, one on each side of the pore and no direct interaction is expected between further molecules added and the walls. As we will see below, the excess of adsorbed hydrogen actually reaches limit around 6.5–7 Å and decreases for larger pores. Fig. 2 shows excess hydrogen adsorption isotherms as a function of the hydrogen pressure applied [0, 400 bar]. The maximum storage observed is 0.5 %wt, similar to the values typically obtained for graphite. With increasing pore size, hydrogen storage capacity improves until the optimum pore size of 6.5 Å, being reduced for larger pore widths. The most efficient response is achieved for the 6.5 Å pore graphite, which can store up to ca. 2.25 %wt in excess at 300 bar pressure. This is in agreement with previous theoretical and experimental studies [10–21].

Particularly, the 9.0 and 10.0 Å wide pores present curves with a pronounced adsorption increase at 150 bar, whereas at low pressures the slopes of these curves are still lower than those observed for smaller pores. This effect can be observed in the inset of Fig. 2. While in the 5.5 Å pore the isotherm slope is 0.0024 %wt_H_2/bar, the optimum pore for adsorption of hydrogen (6.5 Å) presents a slope of 0.023 %wt_H_2/bar (an order of magnitude greater), and in the pore of 10.0 Å it drops to 0.015 %wt_H_2/bar.

Fig. 3 shows the curve for hydrogen densities as a function of distance from the center of the pore. As pore size increases from 5.5 Å to 6.5 Å, the curve becomes higher and wider, a fact which is in agreement with the increase in the storage capacity observed in Fig. 2. In the case of 7.0 Å and 7.5 Å pore sizes, the curves decrease in height and increase in width. For the 9.0 and 10.0 Å pores, the hydrogen density curves show clearly two peaks, indicating the formation of bilayers.

3.2. Oxygen adsorption

In a previous work [7–9], we found that the main interferent for hydrogen storage is oxygen, due to the fact that this molecule competes for the same adsorption sites, but with a stronger binding. For this reason, we have also studied oxygen adsorption in porous graphite. In the case of the oxygen molecule, we also considered pores in the [5.5 Å, 14.0 Å] range. The reasons for this choice are the same as those discussed above for the case of hydrogen. From these simulations, it was found that

Table 2 – Nomenclature of the model isotherm parameters.

P_c	Highest charging pressure upon loading of the tank (right after charging at the external pressure).
P_d	Lowest discharge pressure.
P	Total pressure (before loading).
$P^{c.Eq}$	Total pressure in charge balance (at equilibrium).
P_{H_2}	Partial pressure of hydrogen.
P_{O_2}	Partial pressure of oxygen.
ΔP_{H_2}	Variation of hydrogen pressure in charging process.
ΔP_{O_2}	Variation of oxygen pressure in charging process.
$P^{c.Eq}_{H_2}$	Hydrogen charge pressure in gas phase when system reaches equilibrium.
$P^{c.Eq}_{O_2}$	Oxygen charge pressure in gas phase when system reaches equilibrium.
γ_{H_2}	Hydrogen purity of mixture introduced into the tank.
V	Dead volume corresponding to a portion of the total volume of the reservoir for hydrogen storage.
$n^T_{H_2}$	Total number of hydrogen molecules.
$n^T_{O_2}$	Total number of oxygen molecules.
$n^g_{H_2}$	Number of hydrogen molecules in gas phase.
$n^g_{O_2}$	Number of oxygen molecules in gas phase.
$n^s_{H_2}$	Number of hydrogen molecules in the adsorbed phase.
$n^s_{O_2}$	Number of oxygen molecules in the adsorbed phase.
R	Universal gas constant.
T	Temperature.
α_{H_2}	Hydrogen constant in Langmuir isotherm for competitive adsorption.
α_{O_2}	Oxygen constant in Langmuir isotherm for competitive adsorption.
N_T	Total number of adsorption sites in the adsorbent.
n_u	Empty sites in the adsorbent.
Δn_{H_2}	Number of hydrogen moles that are introduced in charging process.
Δn_{O_2}	Number of oxygen moles that are introduced in charging process.
dn^{out}_T	Quantity of hydrogen and oxygen that exist in the tank at infinitely slow discharge process.
$dn^{out}_{H_2}$	Quantity of hydrogen that exist in the tank in infinitely slow discharge process.
$dn^{out}_{O_2}$	Quantity of oxygen that exist in the tank in infinitely slow discharge process.

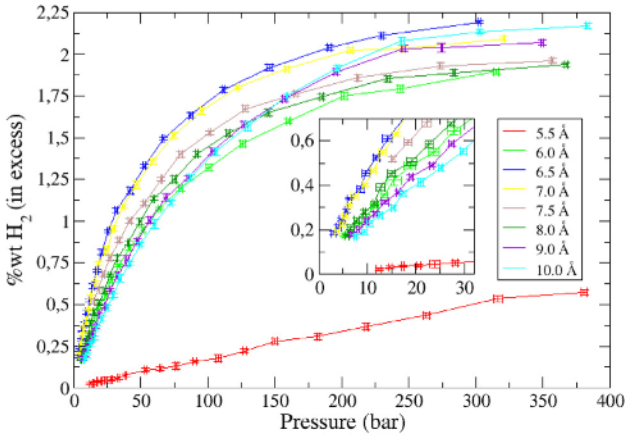

Fig. 2 – Excess adsorption isotherms for H_2 at 300 K in idealized graphite slit pores of different sizes. Inset: magnification in the range of 0–30 bar, which corresponds to 0 to 0.7% wt H_2 in excess.

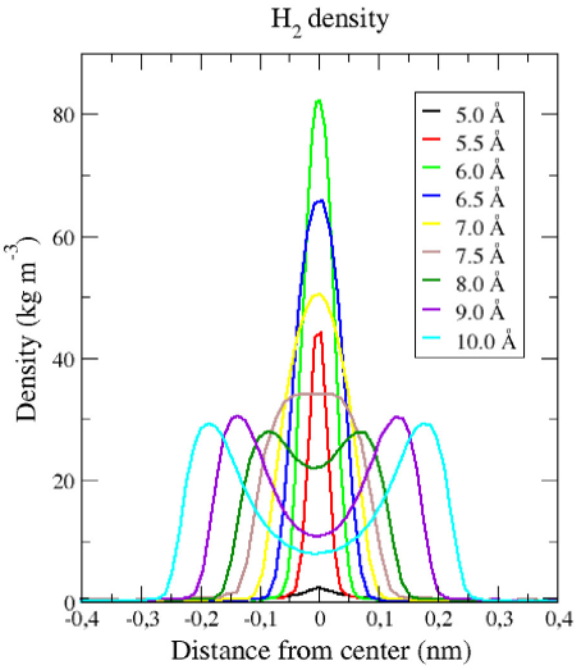

Fig. 3 – Variation of H_2 density inside the different graphite slit pores at 300 K. Pore widths are given in the figure inset.

oxygen was unable to penetrate the 5.5 Å pores under our simulation conditions. Fig. 4 shows adsorption isotherms for oxygen. In the case of 6.0 Å pores, the slope of the isotherm curve is of 2.9 %wt_O_2/bar, saturating at 20 %wt excess in O_2 at ca. 100 bar. In the range of 6.5–7.5 Å, adsorption curves exhibit a relatively high slope at low pressures, in the order of 7–8 % wt_O_2/bar, reaching the saturation region at pressures close to 40 bar, showing storage capacities of 30 %wt O_2. Graphite pores of 8.0 and 9.0 Å present adsorption curves with a transition behavior between the smaller and greater pores, and slopes of ca. 5 %wt_O_2/bar. On the other hand, graphite with wider pores

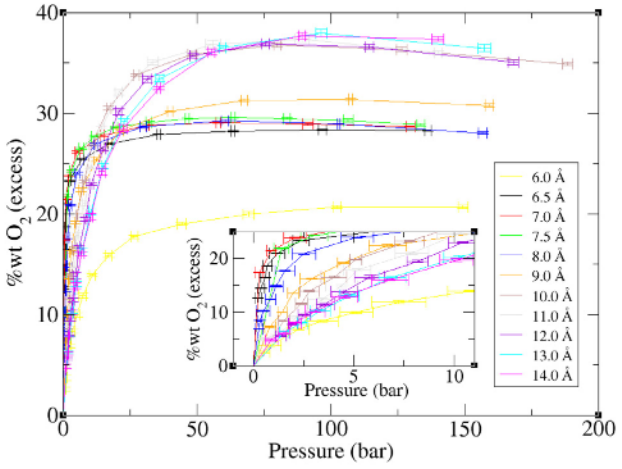

Fig. 4 – Excess adsorption isotherms for O_2 at 300 K in idealized graphite slit pores of different sizes. Inset: magnification from 0 to 10 bar, and from 0 to 25% wt O_2 in excess.

in the range of 10.0–14.0 Å, exhibits the lowest slopes at lower pressures (2.5 %wt_O_2/bar on average), reaching saturation at higher pressures, ca 60 bar. In this case the amount of excess O_2 is 35% wt, that is larger than before.

Comparison between previously differentiated groups of curves is analogous to the case of hydrogen we have already examined. As shown in Fig. 5, from 8.0 to 9.0 Å separations an oxygen double layer is formed between the graphite sheets; and from 13.0 to 14.0 Å pores there begins the formation of a third adsorption layer.

3.3. *Hydrogen storage as a function of the number of cycles*

Adsorption curves of hydrogen and oxygen corresponding to 6.5 Å and 10 Å pores were fitted to Langmuir isotherms, resulting in the α_{H_2} and α_{O_2} values reported in Table 3.

A 6.5 Å pore width was chosen due to the fact that this is an optimum size for the hydrogen storage capacity (Fig. 2). Particularly, this pore size is the one presenting the steepest isotherm curves for the low pressure region for oxygen, as shown in Fig. 4. On the other hand, the 10 Å pore width corresponds to the largest pore size studied for hydrogen in which a double layer is formed, and where the slope of the oxygen curve for low pressures is lower.

From the α_{H_2} and α_{O_2} values reported in Table 3 and using Equation (4) to get $n^s_{H_2}/n^s_{O_2} - \alpha_{H_2}/\alpha_{O_2}P_{H_2}/P_{O_2} - \alpha_{H_2}/\alpha_{O_2}n^g_{H_2}/n^g_{O_2}$, we see that the adsorbed phase will be enriched in oxygen by a factor close to 50–100 with respect to the gas mixture, depending on pore size.

With this information, and the modeling presented in Section 2.2, oxygen enrichment by the adsorbent as a function of the number of charge/discharge cycles was calculated.

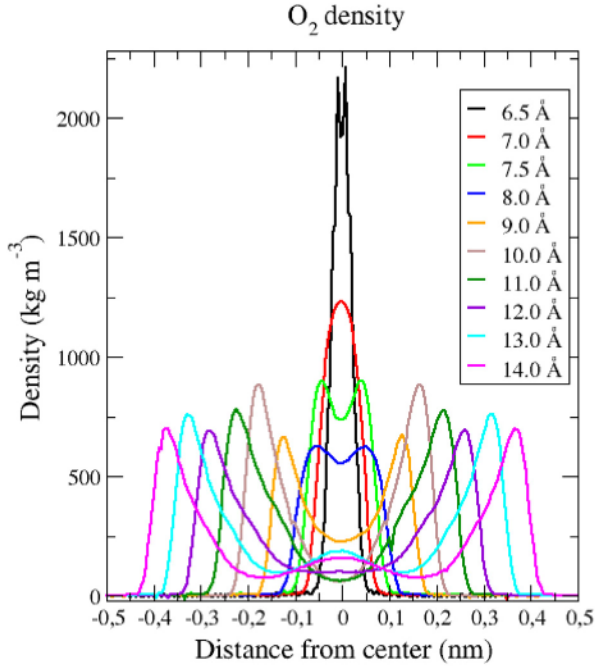

Fig. 5 – Variation of O_2 density inside the different graphite slit pores at 300 K.

Table 3 – α_{H_2} and α_{O_2} Langmuir parameters fitted from molecular dynamics simulations for two different pore sizes.

	α_{H_2} (1/bar)	α_{O_2} (1/bar)
6.5 Å	0.021	2.478
10.0 Å	0.037	1.214

The results are shown in Fig. 6 for different purities of the incoming hydrogen mixture, namely γ_{H_2} – 95%, 99%, 99.9%.

For the optimum pore size for hydrogen adsorption (6.5 Å) and a purity of the incoming gas of 99.9%, about 10% of the adsorption sites become blocked by oxygen after ca. 50 cycles. In contrast, in the case of the 10.0 Å pores and for the same purity of charging gas, the limiting blockage by oxygen drops to ca. 2%. Although it sounds paradoxical that the pores more suited to store hydrogen become more easily blocked by oxygen, the reason for this behavior is to be found in Langmuir parameter α. At low pressures, which are the conditions operative for oxygen in the present system, this parameter determines the slope of the isotherms, thus favoring oxygen adsorption according to the values reported in Table 3. The situation worsens for low-purity hydrogen supply, where oxygen blockage may reach values as large as 15% and 17% in the case of 99% and 95% hydrogen purity respectively, considering the 6.5 Å pore width absorbent. While for the present hydrogen system oxygen blockage appears as a minor hindrance, this effect could become critical in other materials, such as those where metal decoration has been proposed as a way to improve hydrogen storage in carbonaceous materials. In fact, first principles calculations have shown that oxygen may become a major competitor of hydrogen in metal/graphitic systems [7–9].

4. Conclusions

In this work we have presented a new model to analyze the progressive blockage of a hydrogen storage material by oxygen adsorbed species. Specific calculations were performed for a model system, consisting of porous graphite, represented by graphene sheets with different spacing between them.

Molecular dynamics simulations were used to determine adsorption isotherms for hydrogen and oxygen that were fitted to Langmuir-like isotherms.

For optimum pore size for hydrogen adsorption and a purity of 99.9% for the incoming gas, the blockage of active sites by oxygen, at ~50 cycles of charge/discharge, is of 10%. In contrast, in 10.0 Å pores and for the same purity of the charging gas, the tank is blocked by oxygen at 2%. Storage capacity is found to be strongly dependent on the purity of the input mixture.

To the best of our knowledge, the present one is the first attempt to model increased blockage of an adsorbent for hydrogen adsorption by a co-adsorbate upon repetitive charge/discharge cycling of the system. For the present adsorbent, the results show that oxygen is a relatively weak competitor of hydrogen. However, according to the DOE (USA) target criteria of on-board hydrogen storage (room temperature, moderate pressure and high hydrogen uptake), metal-decorated carbon may be a potential way to store hydrogen rather than the purely porous carbons. On the basis of our previous work related to hydrogen adsorption on metal-carbon systems [7–9] we expect this effect to be dramatic for these adsorbents. In order to extend the present model to these systems, careful fitting of hydrogen metal (carbon) interaction potentials is required and will be addressed in future work.

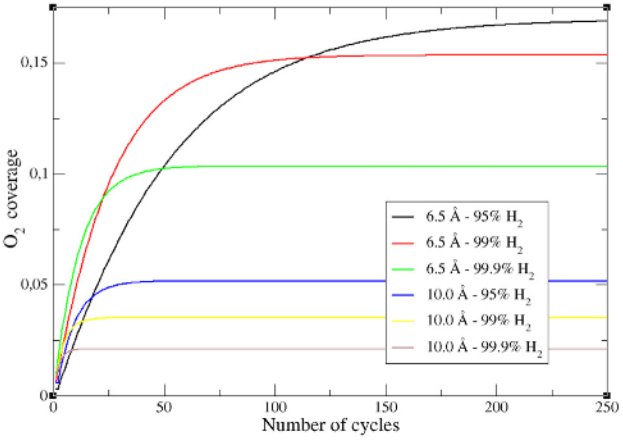

Fig. 6 – Change of excess hydrogen storage capacity as a function of the number of loading/unloading cycles. Gaseous mixtures of hydrogen and oxygen which are introduced into the storage device; hydrogen purities are reported in the inset.

Acknowledgments

This work was supported by PIP 11420090100066 CONICET, FONCyT PICT-2012-2324SECyT UNC, CCAD-UNC and GPGPU Computing Group, Argentina. A. Sigal wishes to thank SECyT UNC for the doctoral fellowship.

REFERENCES

[1] Tollefson J. Hydrogen vehicles: fuel of the future? Nature 2010;464:1262.
[2] Xu WC, Takahashi K, Matsuo Y, Hattori Y, Kumagai M, Ishiyama S, et al. Investigation of hydrogen storage capacity of various carbon materials. Int J Hydrogen Energy 2007;32:2504.
[3] Züttel A. Materials for hydrogen storage. Mater Today 2003;18-27.
[4] Dillon AC, Jones KM, Bekkedahl TA, Kiang CH, Bethune DS, Heben MJ. Storage of hydrogen in single-walled carbon nanotubes. Nature 1997;386:377–9.
[5] López-Corral I, Germán E, Juan A, Volpe MA, Brizuela G. DFT study of hydrogen adsorption on palladium decorated graphene. J Phys Chem C 2011;115:4315–23.
[6] Felten A, Suarez-Martinez I, Ke X, Van Tendeloo G, Ghijsen J, Pireaux JJ, et al. The role of oxygen at the interference between titanium and carbon nanotubes. Chem Phys Chem 2009;10:1799–804.
[7] Rojas MI, Leiva EP. Density functional theory study of a graphene sheet modified with titanium in contact with different adsorbates. Phys Rev B 2007;76:155415.

[8] Sigal A, Rojas MI, Leiva EPM. Interferents for hydrogen storage on a graphene sheet decorated with nickel: a DFT study. Int J Hydrogen Energy 2011;36:3537–46.
[9] Sigal A, Rojas MI, Leiva EPM. Is hydrogen storage possible in metal-doped graphite 2D systems in conditions found on Earth? Phys Rev Lett 2011;107:158701.
[10] Oliveira LFL, Laref S, Mayousse E, Jallut C, Franco AA. A multiscale physical model for the transient analysis of PEM water electrolyzer anodes. Phys Chem Chem Phys 2012;14:10215–24.
[11] Oliveira LFL, Jallut C, Franco AA. A multiscale physical model of a polymer electrolyte membrane water electrolyzer. Electrochim Acta 2013;110:363–74.
[12] Cabria I, López MJ, Alonso JA. The optimum average nanopore size for hydrogen storage in carbon nanoporous materials. Carbon 2007;45:2649–58.
[13] Im JS, Park S, Kim TJ, Kim YH, Lee Y. The study of controlling pore size on electrospun carbon nanofibers for hydrogen adsorption. J Colloid Interface Sci 2008;318:42–9.
[14] Kim B, Park S. Optimization of the pore structure of nickel/graphite hybrid materials for hydrogen storage. Int J Hydrogen Energy 2011;36:648–53.
[15] Wang Q, Johnson JK. Molecular simulation of hydrogen adsorption in single-walled carbon nanotubes and idealized carbon slit pores. J Chem Phys 1999;110:577.
[16] Rzepka M, Lamp P, de la Casa-Lillo MA. Physisorption of hydrogen on microporous. J Phys Chem B 1998;102:10894–8.
[17] Texier-Mandoki N, Dentzer J, Piquero T, Saadallah S, David P, Vix-Guterl C. Hydrogen storage in activated carbon materials: role of the nanoporous texture. Carbon 2004;42:2744–7.
[18] García Blanco AA, Alexandre de Oliveira JC, López R, Moreno-Piraján JC, Giraldo L, Zgrablich G, et al. A study of the pore size distribution for activated carbon monoliths and their relationship with the storage of methane and hydrogen. Colloids Surfaces Physicochem Eng Aspects 2010;357:74.
[19] Simon JM, Haas OE, Kjelstrup S. Adsorption and desorption of hydrogen on graphite by molecular dynamics simulations. J Phys Chem C 2010;114:10212–20.
[20] Peng L, Morris JR. Prediction of hydrogen adsorption properties in expanded graphite model and in nanoporous carbon. J Phys Chem C 2010;114:15522.
[21] Gotzias A, Tylianakis E, Froudakis G, Steriotis T. Theoretical study of hydrogen adsorption in oxygen functionalized carbon slit pores. Microporous Mesoporous Mater 2012;154:38.
[22] Kim BH, Hong WG, Moon HR, Lee SM, Kim JM, Kang S, et al. Investigation on the existence of optimum interlayer distance for H_2 uptake using pillared-graphene oxide. Int J Hydrogen Energy 2012;37:14217–22.
[23] Data from the chemistry section of the NIST webbook www.webbook.nist.gov.
[24] Korth M, Pitonák M, Rezác J, Hobza P. A transferable H-bonding correction for semiempirical quantum-chemical methods. J Chem Theory Comp 2010;6:344–52.
[25] Rezác J, Fanfrlik J, Salahub D, Hobza P. Semiempirical quantum chemical PM6 method augmented by dispersion and H-bonding correction terms reliably describes various types of noncovalent complexes. J Chem Theory Comp 2009;5:1749–60.
[26] Bénard P, Chahine R. Determination of the adsorption isotherms of hydrogen on activated carbons above the critical temperature of the adsorbate over wide temperature and pressure ranges. Langmuir 2001;17:1950–5.
[27] Methis David A. Hydrogen technology for energy (energy technology review). USA: Knowledge Publications Corporation; 2007.